**An Acad Bras Cienc (2021) 93(Suppl. 2): e20201606 DOI 10.1590/0001-3765202120201606**
Anais da Academia Brasileira de Ciências | *Annals of the Brazilian Academy of Sciences*
Printed ISSN 0001-3765 I Online ISSN 1678-2690
www.scielo.br/aabc | www.fb.com/aabcjournal

PALEONTOLOGY

# Shell and long-bone histology, skeletochronology, and lifestyle of *Araripemys barretoi* (Testudines: Pleurodira), a side-necked turtle of the Lower Cretaceous from Brazil

MARIANA VALÉRIA A. SENA, RENAN ALFREDO M. BANTIM, ANTÔNIO A.F. SARAIVA, JULIANA M. SAYÃO & GUSTAVO R. OLIVEIRA

**Abstract:** In this study we provide a comprehensive investigation of the microanatomical and microstructural aspects of the carapace and limb bones of the Early Cretaceous side-necked turtle, *Araripemys barretoi*, from the Araripe Basin, Brazil. Inter-elemental histovariability reveals different secondary remodelling of the skeletal elements within the same individual. The vascularisation is scarce and mainly longitudinal, also it ceases towards the bone surface, forming an avascular parallel-fibred bone with closely spaced LAGs. These traits indicate a late ontogenetic stage and a slow growth rate for one of the two *A. barretoi* specimens. The high cortical thickness of the costal plate suggests an increase of the shell stiffness. The elevated relative bone wall thickness of the ulna compared to other limb bones indicates a case of local pachyosteosclerosis, possibly to improve body stability in the aquatic environment.

**Key words:** Araripe Basin, bone histology, Early Cretaceous, shell histology, turtle.

## INTRODUCTION

The turtle shell is formed by the carapace (dorsal portion) and the plastron (ventral portion) connected by lateral bridges, which develop the physical protection of inner soft tissues (Gilbert et al. 2001). In most turtles, keratin scutes overlay the carapace and plastron, which increase the shell's stiffness (Wyneken 2001). Furthermore, shell bones store water and fat besides acting as a pH buffer (Gilbert et al. 2001) and also play a structural role in other behaviours such as support the muscles attached to produce force during locomotion and ventilatory movements during breathing (Landberg 2003, Lyson et al. 2016). Scheyer & Sander (2007) and Jannello et al. (2020) attributed a correlation between shell microanatomy and lifestyle, establishing histological categories to determine crucial features in shell microstructure of Testudines with terrestrial, aquatic non-marine or marine habits. In the last few years, several studies demonstrated that lifestyle influences the shell compactness of these amniotes. For instance, terrestrial turtles exhibit higher compactness indices (Scheyer et al. 2015) than freshwater and marine turtles (Scheyer et al. 2014, Jannello et al. 2016).

The ontogenetic stage of the individuals can be identified through osteohistological studies in vertebrates. Limb bone microstructures have been established as a useful proxy for assessing skeletochronology among recent sea turtle species (e.g. Snover & Hohn 2004, Snover et al. 2011), and in terrestrial and freshwater Testudines (e.g. Chinsamy & Valenzuela 2008,

Botha & Botha 2019). These investigations validate the annual periodicity of rapid and slow bone apposition, and periods of complete cessation of bone deposition in this group of vertebrates.

Among fossil turtles, the Araripemydidae is an extinct pleurodiran clade known mainly from deposits of the Santana Group in the Araripe Basin (Meylan 1996, Oliveira & Kellner 2017, Limaverde et al. 2020). *Araripemys* is one of these taxa and is considered an aquatic turtle living during the Early Cretaceous environment of Gondwana (Oliveira & Romano 2007). The taxon is the only turtle recorded in two distinct lithostratigraphic units of the Santana group: Crato and Romualdo formations (Oliveira et al. 2011, Carvalho & Barreto 2015, Oliveira & Kellner 2017), showing a higher tolerance for living in environments with different salinity levels (Oliveira & Kellner 2017). The Santana Group yielded a broad Testudines fauna from the Early Cretaceous, represented by five monotypic genera to date. Except for *Santanachelys*, all of them belong to Pleurodira (Romano et al. 2013). This diversity of body shape and environmental tolerance of pleurodirans allows for an ideal setting for studies of an osteohistological nature. Herein we present results of histological and microanatomical analyses of two costal plates, one neural plate, one peripheral plate, both humeri, one ulna, one radius and metatarsals of two specimens of *Araripemys,* from two geological units of the Santana Group, and compare them with other pleurodiran turtles, to test a correlation between its shell microstructure and lifestyle. In addition, their ontogenetic stage was estimated, using standard skeletochronology methods.

### Institutional abbreviations

MPSC, Museu de Paleontologia Plácido Cidade Nuvens; UFRPE, Universidade Federal Rural de Pernambuco.

## GEOLOGICAL SETTING

The Santana Group of the Araripe Basin is subdivided from base to top into four formations: Barbalha (formerly Rio da Batateira Formation), Crato, Ipubi and Romualdo (Assine et al. 2014). The timing for this Group varies and some studies indicate an Aptian-Albian stage (Benigno et al. 2021). Contrastingly, Arai & Assine (2020) suggested an Aptian age attributed by the presence of the guide palynomorph, *Sergipea variverrucata* in all formations of Santana Group.

The Crato Formation mainly consists of micritic laminated grey and light-beige limestones with halite pseudomorphs. The laminated limestones are interbedded with a series of claystones, siltstones and sandstones and the presence of halite pseudomorphs in some levels indicates deposition under fluctuating salinity levels (Neumann et al. 2003, Martill et al. 2007). Except for the report of the presence of marine foraminifera by Arai M. (unpublished data), the carbonate section is attributed to transgressive-regressive events associated with the expansion and contraction of a lacustrine system (Neumann V.H., unpublished data).

The Romualdo Formation represents a transgressive-regressive complete cycle (Assine et al. 2014). This formation is composed of a wide range of lithologies, including stratified conglomerates, fine to medium grained sandstones, interbedded shales, marls and limestones, and coquinas, which includes the highly fossiliferous carbonate concretion-bearing unit (Valença et al. 2003, Kellner et

al. 2013, Assine et al. 2014, Almeida-Lima et al. 2020, Melo et al. 2020). Despite there being a consensus on its predominantly marine origin, several palaeoenvironment proposals have been made for this sequence. It has been previously interpreted as an estuarine environment (Silva Santos & Valença 1968), as a gulf connected with an open sea (Valença et al. 2003) or even as a non-marine deposit (Martill 2007). Despite this, a recently integrated study of foraminifera, ostracods and other microfossil data, from the Romualdo Formation, indicates a restricted environment after a brief connection with the sea, since some of these representatives are generally less abundant in open-ocean environments (Melo et al. 2020). While the Santana Group was recently considered to be Aptian in age (Arai & Assine 2020), the presence of certain planktonic foraminifera (*Microhedbergellamini globularis* Zone) point to an upper Aptian age for the Romualdo Formation, refining previous information (Melo et al. 2020).

## MATERIALS AND METHODS

### Material

The studied sample includes a fourth and a fifth costal plate, a fifth neural plate, a peripheral plate, metapodials (metatarsals), stylopodials (humeri) and zeugopodials (ulna and radius) corresponding to two individuals (Fig. 1). The first individual UFRPE 5302 includes a partially preserved carapace and the second specimen MPSC R 010 includes the axial and appendicular skeleton associated with a complete shell. Thin sections used in the current study are housed in the histological collection at the Department of Biology of the Universidade Federal Rural de Pernambuco. The specimens were referred to *Araripemys barretoi* Price, 1973 according to diagnostic characters: very flat and sculptured carapace in which first costals reach shell margin between nuchal and first peripherals; the carapace forms fontanelles between the costal and the peripheral plates; the epiplastra are long and narrow with long medial contact to the hyoplastra; the reduced plastron lacks mesoplastra and gular scutes; the entoplastron has an inverted V shape; the epiplastra present a J shape and form a point anteriorly and three midplastral fontanelles; hyoplastra and hypoplastra are nearly rectangular with broadly interdigitating sutures on the midline; and the xiphiplastra have deeply interdigitating sutures with the hypoplastra (Price 1973, Meylan 1996, Oliveira & Kellner 2005).

### Sampling methods

For histological analysis the specimens were hand-measured and photographed as per protocols proposed by Lamm (2013). Samples were removed from each bone element to prepare the histological slides. Thin sections were then prepared using standard fossil histology techniques (Chinsamy & Raath 1992, Scheyer et al. 2007) at the Laboratório de Paleobiologia e Microestruturas (LAPAMI) of the Universidade Federal de Pernambuco (CAV/UFPE) and at the Laboratório de Paleontologia & Sistemática of the Universidade Federal Rural de Pernambuco (LAPASI/UFRPE). The specimens were embedded in clear epoxy resin Resapol T-208, catalysed with Butanox M50 and cut with a diamond-tipped blade mounted on a saw. The mounting side of the sections was wet-ground using a metallographic polishing machine (Aropol-E, Arotec Ltda) with Arotec abrasive sandpapers of increasing grit size (60/P60, 120/P120, 320/P400, 1200/P2500) until a 60 µm thick section be reached.


**Figure 1.** (Colour online) Selected bone elements of *Araripemys barretoi* specimens from Santana Group of the Araripe Basin before sectioning. A, Carapace (UFRPE 5302). B and C, Shell (MPSC R 010). D, Humerus associated with the ulna and radius (MPSC R 010). E, Distal portion of the humerus (MPSC R 010). F, Ulna and radius (MPSC R 010). G, Left pes (MPSC R 010). The dashed lines indicate the histological section planes. Scale bars represent 0.5 cm (e and g); and 1 cm (a, b, c, d and f).

## Histological analyses

Samples were observed using two petrographic polarising microscopes under normal and polarised light with lambda waveplate. Images were obtained using an AxioCam digital sight camera (Zeiss Inc., Barcelona, Spain) mounted to an Axio Imager.M2 (Zeiss Inc. Barcelona, Spain) and an Olympus BX51 (Olympus Corporation, Tokyo, Japan), mounted to an Olympus DP26 (Olympus Corporation, Tokyo, Japan). The images were taken at the Laboratório de Gemologia (UFPE) and at the Laboratório Integrado de Tecnologia em Petróleo, Gás e Biocombustíveis (LITPEG).

Bone compactness analysis was done on all bone elements. The photographs of the cross-sections were transformed into binary images, using Adobe Photoshop® CS6. This method marks the bone tissue in black and vascular spaces (medullary cavity, vascular canals and resorption cavities) in white. The binary images (Supplementary Material – Figure S1) were

quantitatively analysed with the software Bone Profiler, Windows-based version 4.5.8 (Girondot & Laurin 2003) to infer bone compactness of the bone sections. The bone wall thickness measurements were made using Fiji (ImageJ) Software (Schindelin et al. 2012) and the relative bone wall thickness (RBT), that is, the mean thickness of the cortical bone wall divided by the mean diameter of the total bone (Botha & Chinsamy 2004, Bhat et al. 2019), was calculated manually. For the shell bones, the terminology "external cortex" is adopted to the areas towards

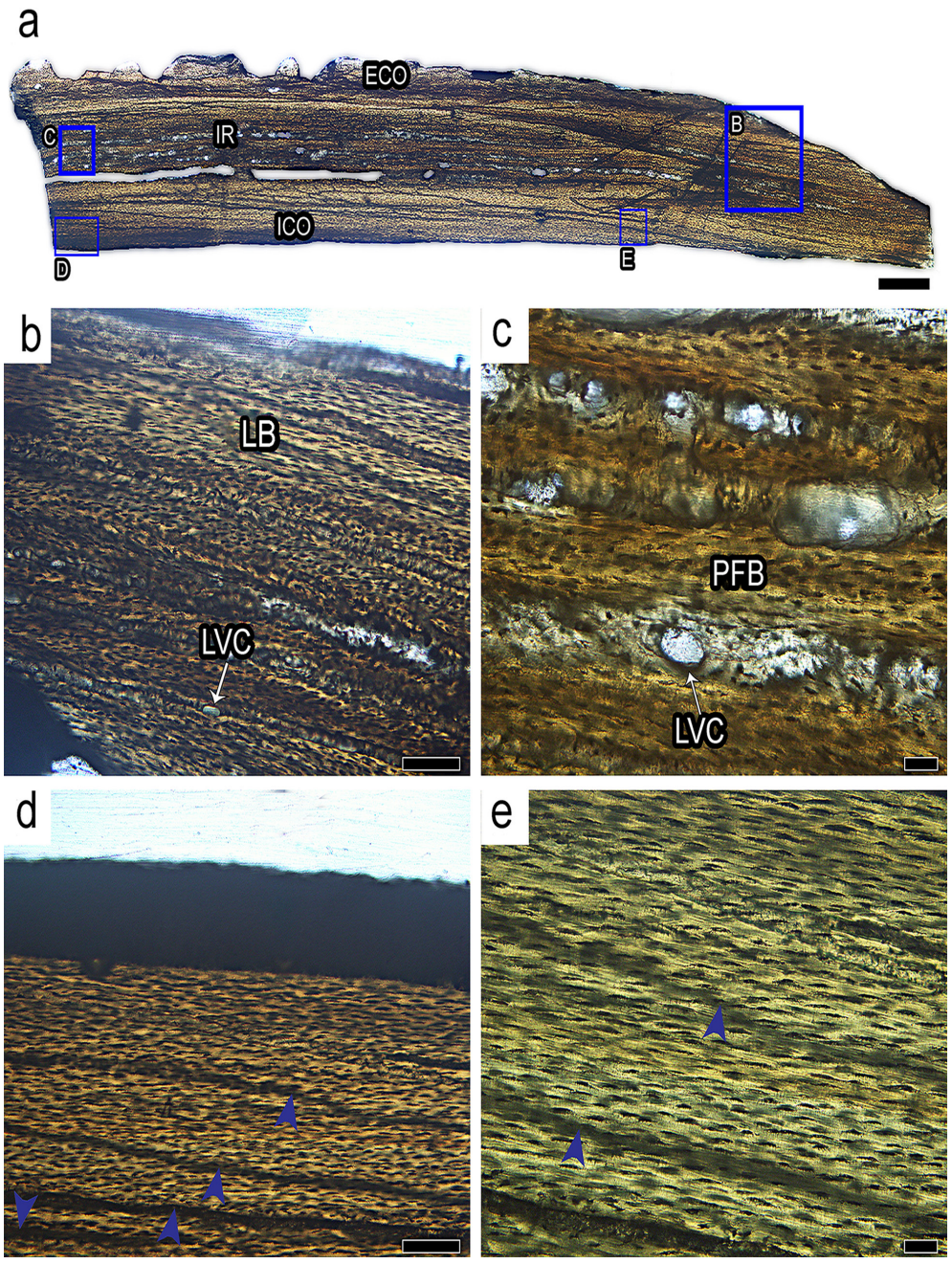


**Figure 2.** (Colour online) Histological section of costal IV plate of *Araripemys barretoi* (UFRPE 5302) from Crato Formation, Lower Cretaceous. A, Microanatomical overview of the perpendicular section of the costal IV plate. B, Detail of the composition of the external cortex. C, Detail of the inner region with reduced vascular spaces. D–E, Cortical bone of the costal composed of parallel-fibred bone tissue interrupted by annuli. Images: Normal transmitted light. Abbreviations: Blue arrowhead, Annulus; ECO, External cortex; ICO, Internal cortex; IR, Inner region; LVC, Longitudinal vascular canal; and PFB, Parallel-fibred bone tissue. Scale bars represent 1 mm (a); 200 µm (b and d); and 5 µm (c and e).

external surface of the bone, whereas "internal cortex" corresponds to the visceral surface of the bone.

## RESULTS

### Histological description

#### *UFRPE 5302*

*Costal IV*. Both external and internal cortices show similar histology (Fig. 2a-e). Primary bone mainly consists of lamellar bone tissue grading to parallel-fibred bone tissue. Lamellar bone tissue shows several osteocyte lacunae with a flatter and elongated appearance following a parallel arrangement towards the surface than the parallel-fibred bone tissue. The latter is composed of intrinsic fibres oriented parallel to the surface interrupted by thick and dark growth marks with a reduced amount of osteocyte lacunae interpreted as annuli (Fig. 2c–e). Simple vascular canals occur in the external and internal cortices and also infilling the inner region (Fig. 2c).

*Neural V*. The external cortex exhibits parallel-fibred bone tissue. The bone matrix shows an enormous amount of osteocyte lacunae following the orientation of the fibres (Fig. 3c). These lacunae have an elongated aspect in the parallel-fibred matrix and a globular appearance in the woven matrix. Some anastomosed vascular canals opening up to the bone surface and connect with ornamental pits. The inner region presents few and short resorption cavities, and secondary osteons feature the remodelling bone tissue. Some portions present primary bone represented by primary osteons (Fig. 3c and 3d). In its lateral part, the remodelling processes expand into the external cortex. The internal cortex consists of regions of woven and parallel-fibred bone tissues (Fig. 3b and 3d). The vascularisation pattern is formed by primary osteons, anastomosed and longitudinal simple vascular canals.

#### *MPSC R 010*

*Costal V*. The external cortex is broader and more vascularised than the internal cortex (Fig. 4a, Supplementary Material – Figure S1). The woven bone tissue has dispersed osteocyte lacunae. The vascular meshwork has a reticular and longitudinal pattern (Fig. 4e). The inner region is occupied by cancellous bone represented by short resorption cavities and secondary osteons. In the central core of the costal plate (in parallel section) occurs the largest circular cavity (Fig. 4b). The internal cortex consists of parallel-fibred bone tissue interrupted by growth marks (Fig. 4c and 4g). The vascularisation pattern is composed of scarce primary vascular canals (Fig. 4d).

In the perpendicular section, the costal plate presents as a massive element formed by parallel-fibred bone tissue (Fig. 4h). In this bone tissue, the osteocyte lacunae show a flattened aspect following the orientation of the fibres. The diploë structure is only observed in the most medial part of the plate (Fig. 4f).

*Peripheral*. This plate presents a diploë structure (Fig. 5a). Both cortices are composed of parallel-fibred bone tissue and they have a similar thickness (Fig. 5c). Osteocyte lacunae show a flattened appearance following the orientation of the fibres. The external cortex is vascularised by longitudinal and reticular oriented vascular canals opening up to the external bone surface (Fig. 5b and 5e). The cancellous bone layer is composed of trabeculae and inter-trabecular spaces (Fig. 5d). The transition region between the internal cortex and the cancellous bone is marked by a resorption line (Fig. 5c). The internal

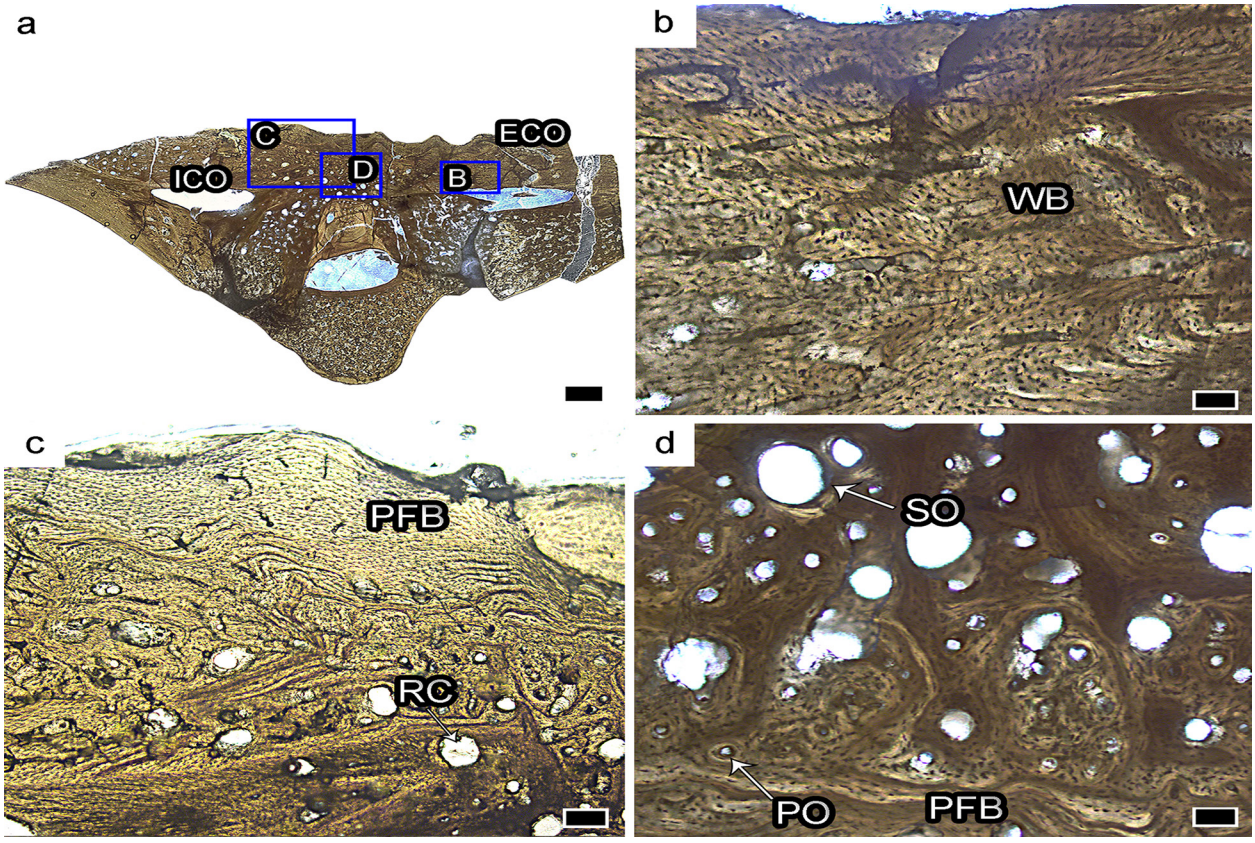


**Figure 3.** (Colour online) Histological section of neural V plate of *Araripemys barretoi* (UFRPE 5302). A, Microanatomical overview of the perpendicular section of the neural V plate. B, The external cortex is composed of woven bone tissue. C, Detail of the external cortex and inner region of the neural plate. D, Remodelling process occurs at the interior region. Images: Normal transmitted light. Abbreviations: ECO, External cortex; ICO, Internal cortex; LB, Lamellar bone tissue; PFB, Parallel-fibred bone tissue; PO, Primary osteon; SO, Secondary osteon; and WB, Woven bone tissue. Scale bars represent 100 µm (a); and 20 µm (b–d).

cortex has its vascular system composed of longitudinal vascular canals.

*Humeri*. The general epiphyseal and metaphyseal microanatomy of the thin sections are similar (Figs. 6a–e and 7a–e). Both cross-sections show a thin region of cortical bone, which surrounds a wide medullary region infilled by cancellous bone (Figs. 6a and 7a). Primary parallel-fibred bone tissues are intercepted by cyclical growth marks (Figs. 6c and 7c). The vascular network is composed of primary longitudinal vascular canals (Figs. 6b and 7d). The medullary region is composed of secondary trabeculae. The walls of the trabeculae are formed by secondary lamellar bone tissue (Figs. 6d–e; 7b and 7e) besides the inter-trabecular spaces are infilled with sedimentary matrix.

*Ulna*. The primary cortex is comprised of parallel-fibred bone with twelve lines of arrested growth (LAGs) (Fig. 8b–c). Cracks have run along some of the LAGs. Primary vascular canals with a longitudinal orientation form the vascularisation pattern. Osteocyte lacunae have a globular or flattened shape; they form

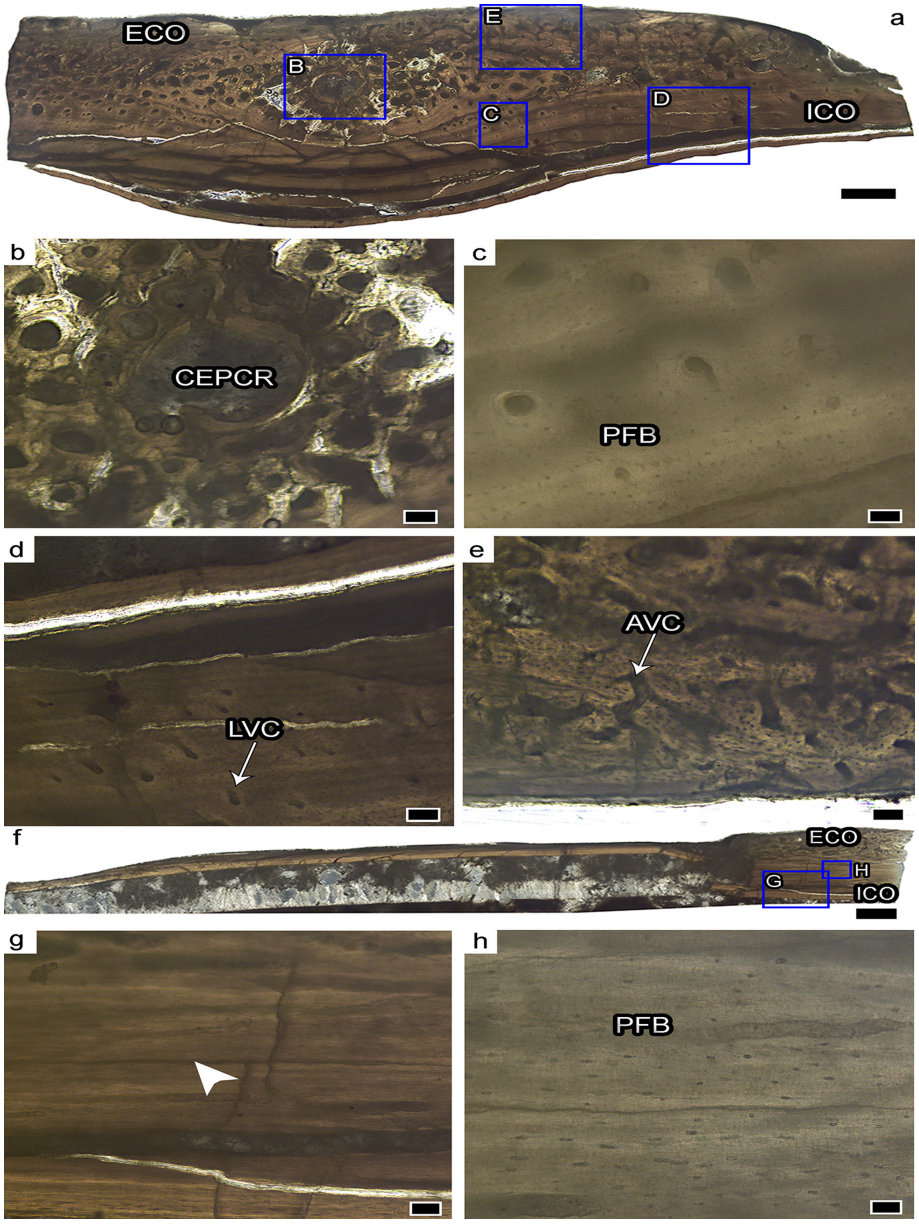


**Figure 4.** (Colour online) Histological section of costal V plate of *Araripemys barretoi* (MPSC R 010) from Romualdo Formation, Lower Cretaceous. A, Microanatomical overview of the parallel section of the costal V plate. B, Centre of embryonic periosteal collar of the rib at the internal region. C and H, internal cortex composed of parallel-fibred bone tissue. D, Longitudinal vascular canals at the internal cortex. E, Anastomosed vascular canals are predominant at the external cortex. F, Microanatomical overview of the perpendicular section of the costal V plate. G, Growth marks are visible in the internal cortex. Images: Normal transmitted light. Abbreviations: AVC, Anastomosed vascular canal; CEPCR, Centre of embryonic periosteal collar of the rib; ECO, External cortex; ICO, Internal cortex; LVC, Longitudinal vascular canal; PFB, Parallel-fibred bone tissue; and White arrowhead, Line of arrested growth. Scale bars represent 300 µm (a); 100 µm (f) and 20 µm (b–e; g and h).

rows following the fibre orientation. Secondary osteons are restricted to the innermost cortex (Fig. 8d). The medullary cavity presents an elongated narrow shape towards the periosteal surface (Fig. 8a).

*Radius*. The primary cortex is composed of parallel-fibred bone tissue interrupted by eleven LAGs and one annulus (Fig. 9b–c). As observed in the ulna, cracks have run along at least two of the LAGs (Fig. 9a). Primary osteons and primary longitudinally-oriented vascular canals constitute the vascularisation pattern (Fig. 9d). Osteocyte lacunae have a globular or flattened aspect dispersed throughout the bone matrix.

*Metapodials*. The overall bone microstructure of the metatarsals consists of primary cortices formed by avascular parallel-fibred bone tissue (Fig. 10a). Metatarsals I and IV exhibit the narrowest and the widest cortices, respectively (Fig. 10b and 10e). Trabecular bone

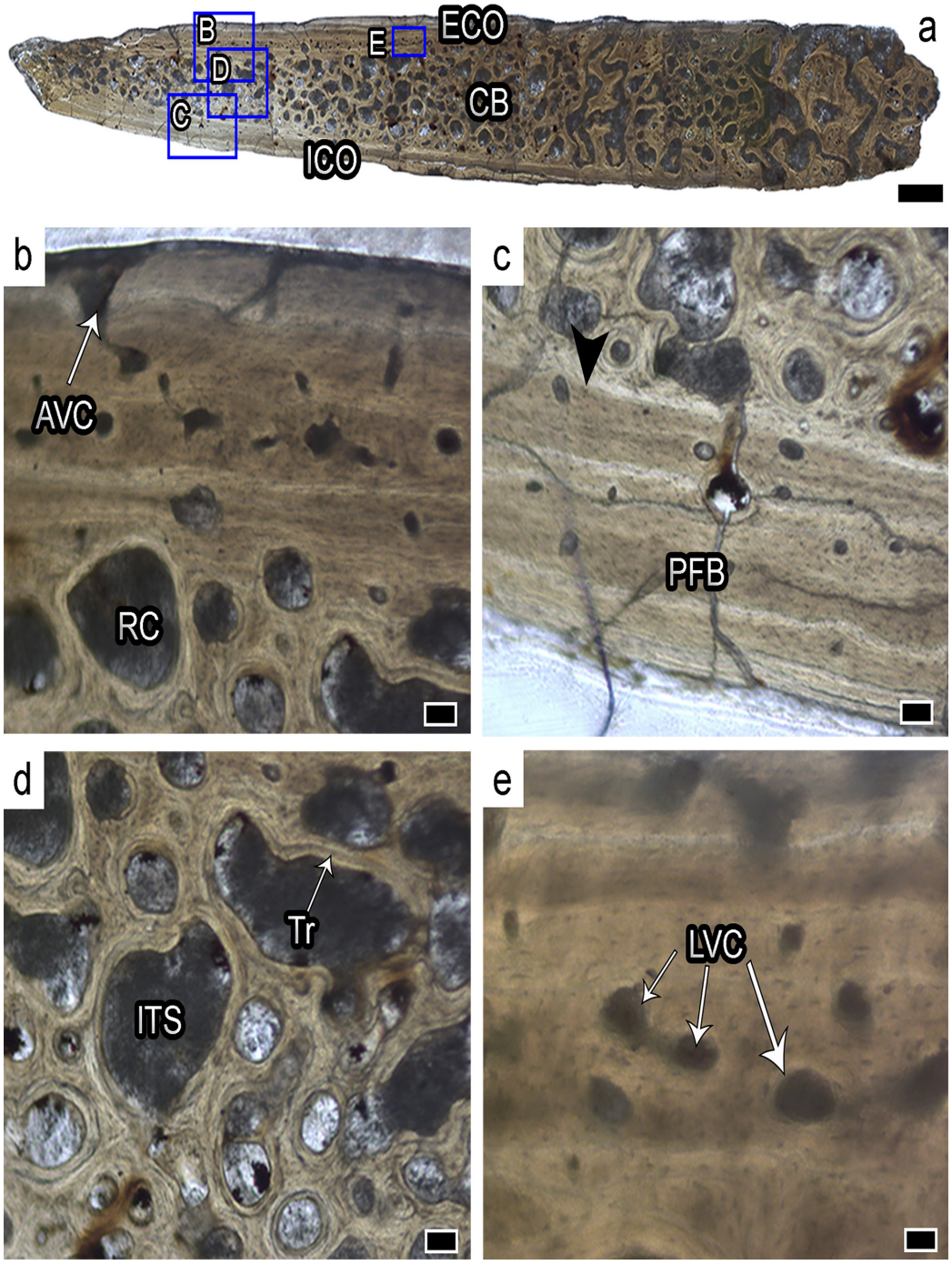


**Figure 5.** (Colour online) Histological section of peripheral plate of *Araripemys barretoi* (MPSC R 010). A, Microanatomical overview of the transverse section of the peripheral plate. B, External cortex with vascular canals opening up to the surface of the bone. C, Limit between the cancellous bone and internal cortex marked by a resorption line. D, Trabeculae forming the cancellous bone layer. E, Longitudinal vascular canals dominate in the external cortex. Images: Normal transmitted light. Abbreviations: AVC, Anastomosed vascular canal; Black arrowhead, Resorption line; CB, Cancellous bone; ECO, External cortex; ICO, Internal cortex; ITS, Inter-trabecular space; LVC, Longitudinal vascular canal; PFB, Parallel-fibred bone tissue; RC, Resorption cavity; and Tr, Trabecula. Scale bars represent 500 µm (a); and 20 µm (b–e).

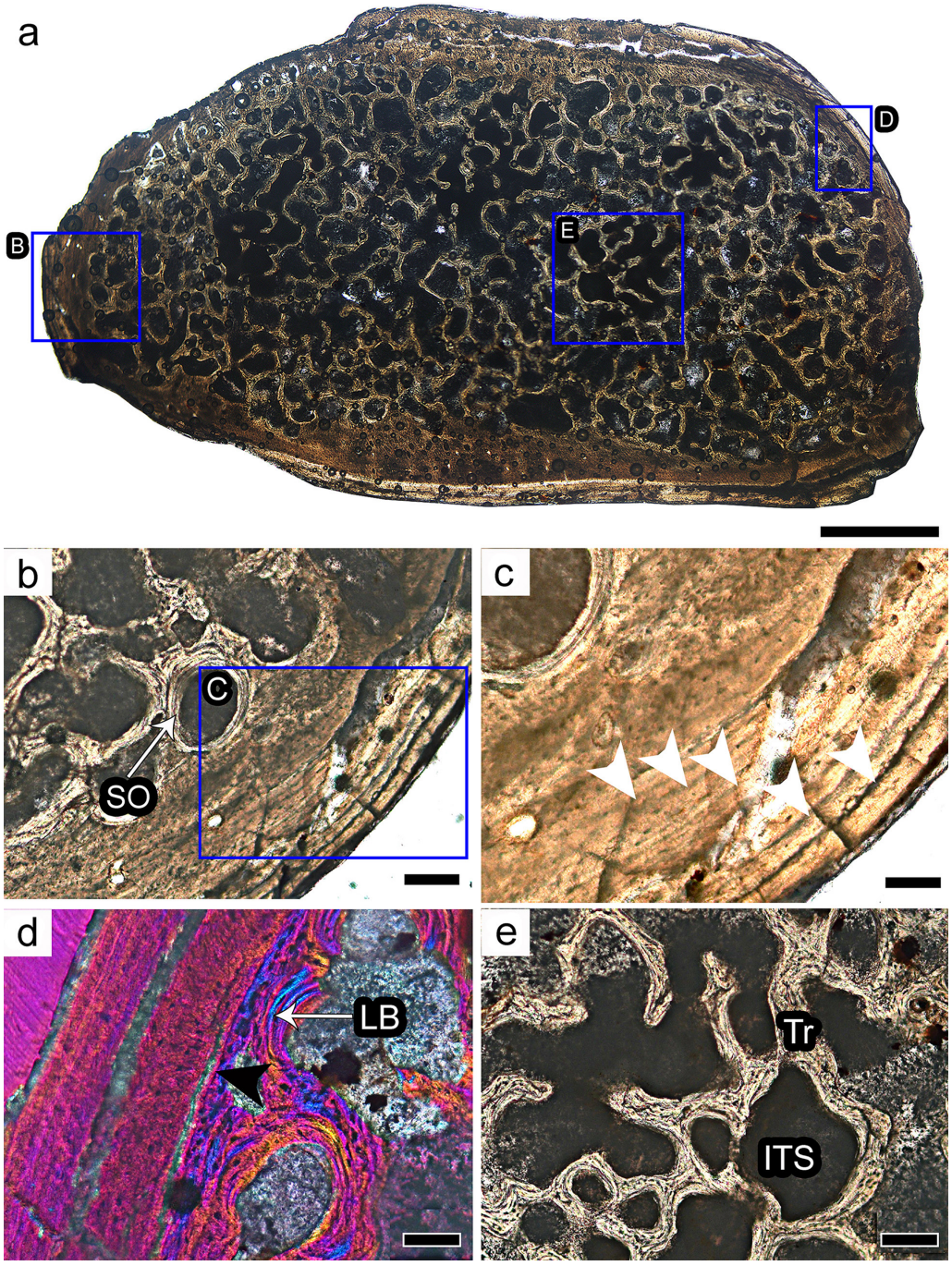


**Figure 6.** (Colour online) Histological section of the humeral epiphysis of *Araripemys barretoi* (MPSC R 010). A, Overall view of an epiphyseal cross-section of the humerus. B, Cancellous bone is dominated by slender bone trabeculae and some secondary osteons. C, Close-up of B showing parallel-fibred cortex interrupted by LAGs. D, Detail of the transition between cortical and cancellous bone demarcated by a thin resorption line. E, Details of the thin lamellar trabeculae of the cancellous bone. Images: Normal transmitted light (a, b, c and e); and Cross-polarised light with lambda waveplate (d). Abbreviations: Black arrowhead, Resorption line; ITS, Inter-trabecular space; LB, Lamellar bone; SO, Secondary osteon; Tr, Trabecula; and White arrowhead, Line of arrested growth. Scale bars represent 1 mm (a); 100 µm (b and e); and 50 µm (c and d).

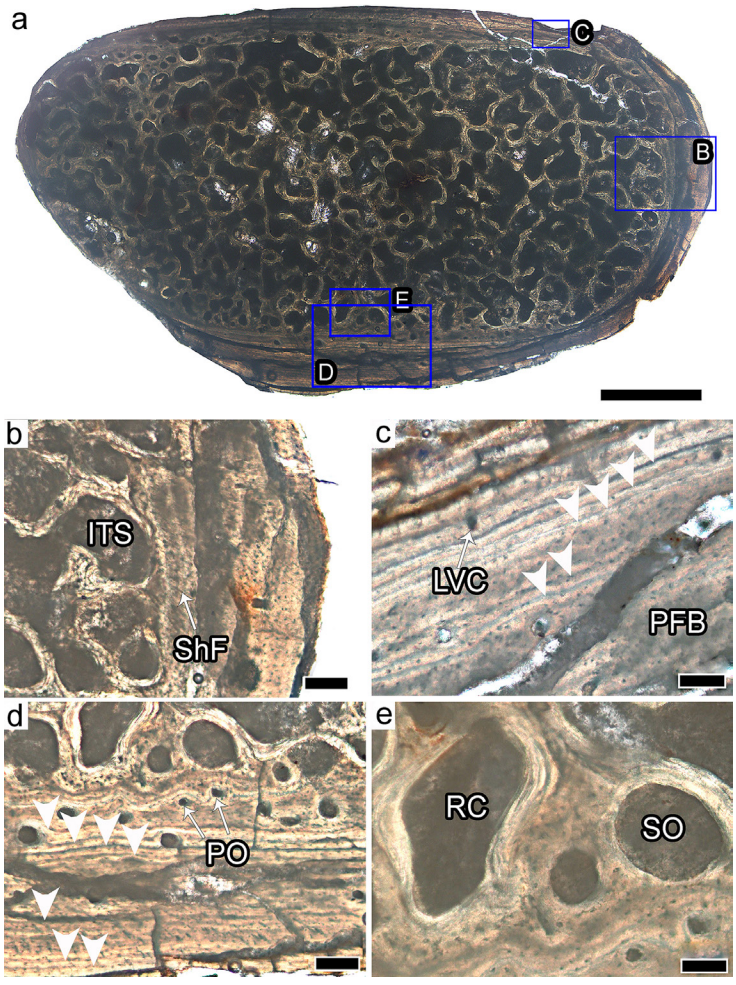


**Figure 7.** (Colour online) Histological section of the humeral metaphysis of *Araripemys barretoi* (MPSC R 010). A, Overall view of a metaphyseal cross-section of the humerus. B, Note the presence of Sharpey's fibres that extend perpendicularly to the bone margins. C, LAGs interrupting parallel-fibred cortical bone. D, Poor vascularised parallel-fibred bone tissue of the periosteal cortex and highly vascularised inner cortex of primary osteons and primary vascular canals. E, Secondary bone remodelling in the perimedullary region. Images: Normal transmitted light. Abbreviations: ITS, Inter-trabecular space; LVC, Longitudinal vascular canal; PO, Primary osteon; PFB, Parallel-fibred bone tissue; RC, Resorption cavity; Shf, Sharpey's fibres; SO, Secondary osteon; White arrowhead, Line of arrested growth. Scale bars represent 1 mm (a); 100 µm (b and d); and 50 µm (c and e).

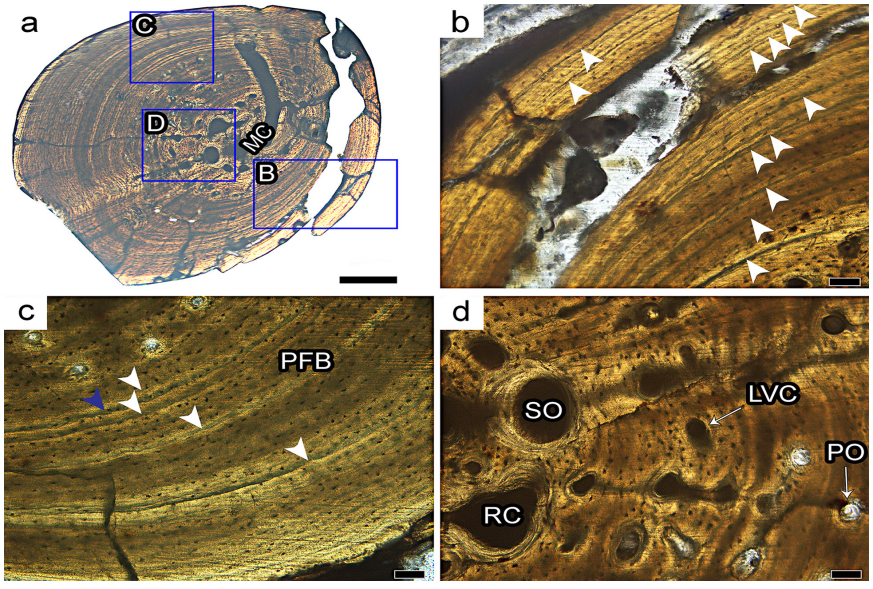


**Figure 8.** (Colour online) Histological section of the ulna of *Araripemys barretoi* (MPSC R 010). A, Overall view of the cross-section of the ulna. B and C, Parallel-fibred cortex interrupted by cyclical growth marks. D, Inner cortex remodelled by secondary osteons and resorption cavities. Images: Normal transmitted light. Abbreviations: Blue arrowhead, Annulus; LVC, Longitudinal vascular canal; MC, Medullary cavity; PO, Primary osteon; RC, Resorption cavity; SO, Secondary osteon; and White arrowhead, Line of arrested growth. Scale bars represent 500 µm (a); and 5 µm (b–d).

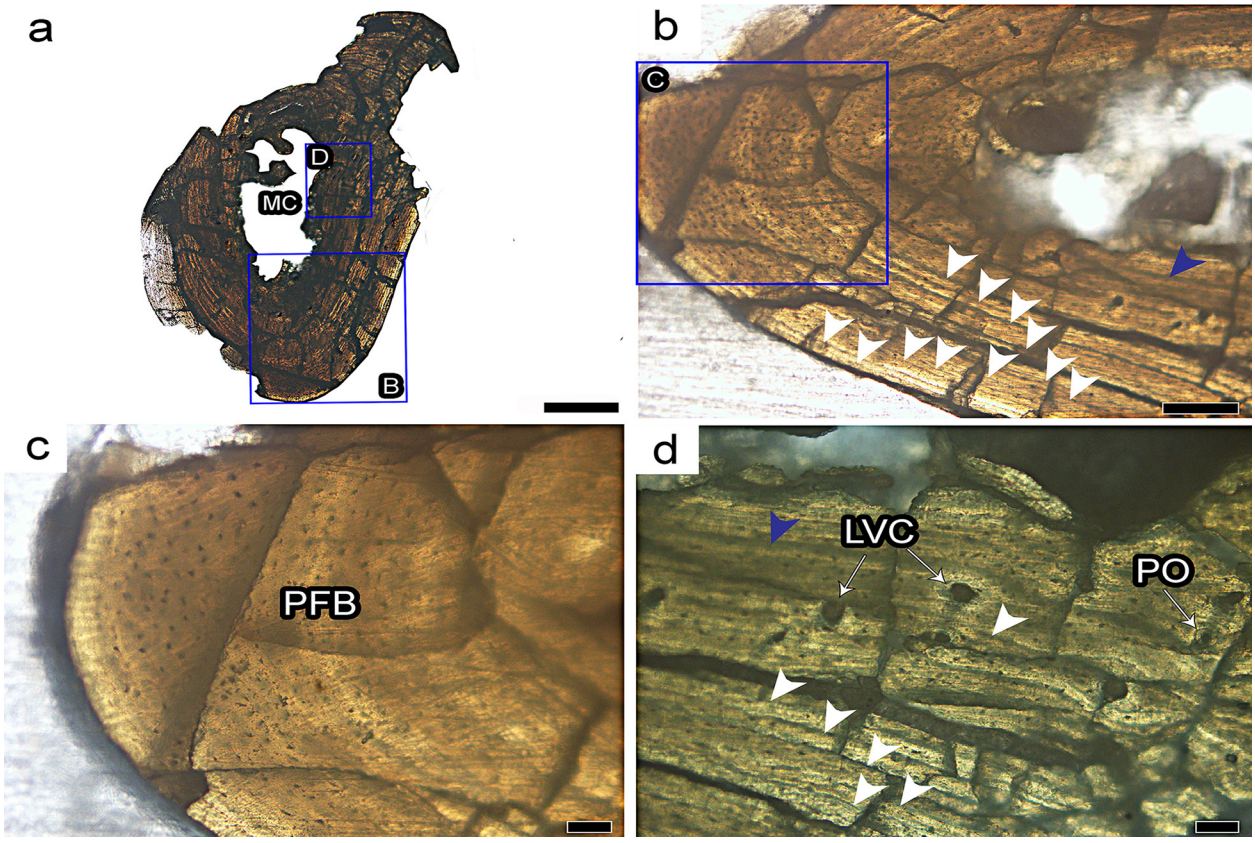


**Figure 9. (Colour online) Histological section of the radius of *Araripemys barretoi* (MPSC R 010). A, Overall view of the cross-section of the radius. B, Cortical bone interrupted by cyclical growth marks. C, Detail of B showing parallel-fibred primary cortex. D, The inner and middle cortex contains several growth marks. Images: Normal transmitted light. Abbreviations: Blue arrowhead, Annulus; LVC, Longitudinal vascular canal; MC, Medullary cavity; PFB, Parallel-fibred bone tissue; PO, Primary osteon; and White arrowhead, Line of arrested growth. Scale bars represent 500 µm (a); 200 µm (b); and 5 µm (c and d).**

and secondary osteons constitute the medullary regions (Fig. 10c). The medullary cavity of metatarsal III is surrounded by convoluted compacted coarse cancellous bone (CCCB), which is separated from the periosteal cortex by a prominent resorption line (Fig. 10d).

## DISCUSSION

### Highly compacted carapace assessment

The most unexpected result of this study was the great difference between osteohistological pattern and palaeoenvironmental data. We used the categories suggested by Jannello et al. (2020) based on Scheyer & Sander (2007) to predict the lifestyle of *Araripemys*. The costal and neural plates present the terrestrial histological type composed of highly compact cortices (Table I) with similar thickness and small vascular canals. In general, the cancellous bone layer is sharply reduced composed by short trabeculae. This shell histology disagrees with the overall lacustrine and marine environment suggested by the sediments where *Araripemys* comes from (Oliveira et al. 2011, Carvalho & Barreto 2015, Oliveira & Kellner 2017). A similar case occurred with the pan-chelid *Rionegrochelys caldieroi* de la Fuente, Maniel and Jannello, 2017 (de la Fuente et al. 2017). This semiaquatic–aquatic species according to its fluvial depositional environment,

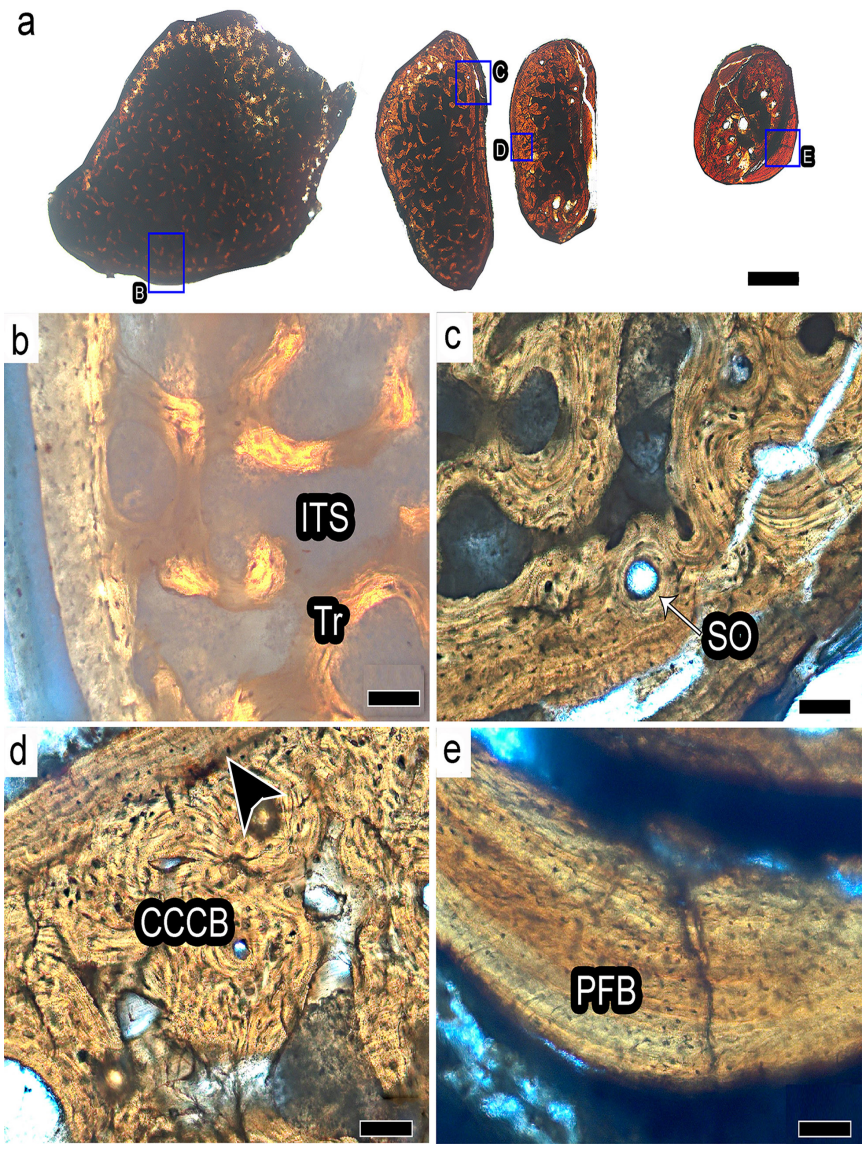


**Figure 10.** (Colour online) Histological section of left metatarsals of *Araripemys barretoi* (MPSC R 010). A, Overall view of cross-sections of the metatarsals. B, Detail of metatarsal I exhibiting thin cortical bone and trabecular bone filling the medullary region. C, Detail of metatarsal II showing the remodelling process in the perimedullary region. D, Detail of metatarsal III showing compacted coarse cancellous bone tissue in the innermost cortex. E, Detail of metatarsal IV displaying parallel-fibred bone tissue in the cortical region. Images: Normal transmitted light. Abbreviations: Black arrowhead, Resorption line; CCCB, Compacted coarse cancellous bone; ITS, Inter-trabecular space; PFB, Parallel-fibred bone tissue; SO, Secondary osteon; and Tr, Trabecula. Scale bars represent 500 µm (a); and 50 µm (b–d).

disagrees with the terrestrial feature revealed by microanatomical features (de la Fuente et al. 2017). In this case, the authors suggested a semiaquatic habit with a tendency to forage in terrestrial environments. Another example is the coastal marine bothremydid, *Cearachelys placidoi*, which also presents a highly compacted plastron (Sena et al. 2021). Thus, the shell bone microstructure may incorrectly predict the palaeoenvironment in which these taxa lived. It is important to record that the costal IV plate has a higher density of osteocyte lacunae which suggests a higher metabolic rate than the appendicular bones sampled.

The absence of LAGs in the UFRPE 5302 costal plate may suggests that annual environmental changes such as seasonal fluctuations in climate, salinity variation and food availability in the Crato palaeolake were not significant to cease the costal growth. Otherwise, this feature may correspond to the early ontogenetic stage for the specimen (Cerda et al. 2014). The possibility of bone resorption erasing the LAGs (Wang et al. 2019) is unlikely because there is

**Table I. Estimated bone compactness and relative bone wall thickness of studied bone elements of *Araripemys barretoi*.**

| Bone element | Min (SE) | Max (SE) | S: slope (SE) | P: transition (SE) | Bone compactness | Relative bone wall thickness (%) |
|---|---|---|---|---|---|---|
| Costal V plate UFRPE 5302 (Perpendicular section) | 91 (n.a) | 91 (n.a) | 5 (n.a) | 50 (n.a) | 0.999 | – |
| Costal V plate UFRPE 5302 (Parallel section) | 91 (n.a) | 91 (n.a) | 5 (n.a) | 50 (n.a) | 0.910 | – |
| Neural V plate UFRPE 5302 | 91 (n.a) | 91 (n.a) | 5 (n.a) | 50 (n.a) | 0.951 | – |
| Peripheral plate UFRPE 5302 | 91 (n.a) | 91 (n.a) | 5 (n.a) | 50 (n.a) | 0.834 | – |
| Humeral epiphysis MPSC R 010 | -4.860085 (0.0052233) | 1122.01 (1.204783) | 15.49973 (0.0017688) | 83.44743 (0.0100576) | 0.511 | 8.4 |
| Humeral metaphysis MPSC R 010 | -4.867664 (0.0025356) | 3735.726 (1.945482) | 10.70954 (0.0008052) | 70.37807 (0.0057536) | 0.682 | 7.82 |
| Ulna MPSC R 010 | 0.9604937 (0.0001777) | -20.59331 (295.3171) | 4.301269 (0) | 97.16246 (0) | 0.96 | 42.98 |
| Radius MPSC R 010 | -0.784116 (0.0004734) | 551.3261 (0.2280387) | 5.822927 (0.0017136) | 34.38055 (0.0118601) | 0.891 | 17.6 |
| Metatarsal I MPSC R 010 | 0.2458498 (0) | 800.1459 (0) | 4.549157(0.0021647) | 33.26039 (0.0197977) | 0.859 | – |
| Metatarsal II MPSC R 010 | -5.601472 (0.0019807) | 449.0123 (0.1584178) | 8.71785 (0.0008965) | 37.76353 (0.0042705) | 0.722 | – |
| Metatarsal III MPSC R 010 | -2.110333 (0) | 576.8223 (0) | 6.235533 (0.0007363) | 33.55287 (0.0045778) | 0.795 | – |
| Metatarsal IV MPSC R 010 | 0.530049 (0) | 272.9994 (0) | 5.981462 (0.0056199) | 39.07308 (0.0416116) | 0.971 | – |

**SE, standard errors.**

no presence of resorption activity such as in *Stupendemys geographicus* Wood, 1976 (Scheyer & Sánchez-Villagra 2007). The presence of annuli in the costal plate might indicate periods of slow growth during unfavorable seasons (Francillon-Vieillot et al. 1990).

The flat external morphology of the carapace plates is reflected in their micromorphology. Most of the carapace is composed of high compacted costal and neural plates. However, the peripheral plate exhibits a cancellous layer more developed that suggests the highest

capacity for acting as a water and waste reservoir within the carapacial plates. The thicker cortices and absence of the diploë structure might be interpreted as serving for the reduction of manoeuvering during swimming, since the presence of the diploë structure of the carapace offers high stiffness and decreasing the weight required for swift swimming (Balani et al. 2011). According to Clarac et al. (2020) massive shells facilitate the turtle's efforts to dive and remain at the bottom of the lake or river. *Araripemys barretoi* was adapted to various salinities of the environmental medium. For example, this species habited the Crato palaeolake, which is characterised as an environment of high salinity and high evaporation rates associated with long dry periods (Martill et al. 2007). The exposition to this euryhaline environment might be compensating by short-term dives, also because of its highly compacted carapace plates; *Araripemys* probably had a low capacity of bone acidosis buffering. Furthermore, a massive carapace contributes to increased shell resistance to compensate for its weakness caused by several fontanelles of the *Araripemys* shell.

Based on a comparison with other fossil and extant turtles, the costal V plate presents an enlarged circular space in the inner region (Fig. 4b). This vascular space was found in *Condorchelys antiqua* and *Heckerochelys romani* being interpreted as the centre of embryonic periosteal collar of the rib early in costal growth (Scheyer et al. 2014, Cerda et al. 2016, Vieira et al. 2016).

## Growth rate, relative bone wall thickness and osseous specialization in limb bones

The cortices of all the limb bones examined exhibit a similar microstructure, suggesting the same growth pattern, represented by parallel-fibred bone tissue with temporary cessation of growth during annual cycles. Humeri show a reduced cortical bone and its medullary regions contain a loose spongiosa like the freshwater cryptodire *Annemys* sp. (Danilov et al. 2018). However, it is not as pronounced as in marine turtles, *Chelonia mydas* (Linnaeus, 1758) (Laurin et al. 2011) and *Dermochelys coriacea* (Vandelli, 1761) (Houssaye 2013). *Araripemys* shares with the tortoises *Chelonoidis carbonaria* (Spix, 1824) and *Homopus femoralis* Boulenger, 1888, highly compacted zeugopodials (Laurin et al. 2011). In this way, high compactness in the ulna and radius might be related to the flat-shelled constraints in *A. barretoi*. Our findings corroborate an earlier study which indicated that turtles with different lifestyles can have similar high compactness indices for the long bones (Kriloff et al. 2008).

Within the limb bones, the coarse cancellous bone (CCCB) only occurs in the perimedullary region of the metatarsal III. This secondary reconstruction decreases the size of the medullary cavity by endosteal compactness of spongy bone (Enlow 1962). The CCCB deposition increases through ontogeny as observed in the stylopodials of the tortoise *Chersina angulata* (Bhat et al. 2019). In long bones with active growth, the metaphyseal region consists of spongy bone (Woodward et al. 2018). During ontogeny the bone shaft elongates, the diaphysis incorporates metaphyseal region and the trabeculae are subsequently infilled with primary bone to form CCCB (Enlow 1963). Given that herein the remodelled CCCB only occurs in one growing metapodial and it is likely related to the metaphyseal position of the section of the third metatarsal.

Inter-elemental variation in the relative bone wall thickness (RBT) is recorded in Table I. The ulna has the highest RBT (42%), suggesting a higher rate of appositional growth relative to the other limb bones and represents a case of pachyosteosclerosis, i.e., the development of hyperplasic periosteal cortical and an increase in inner bone compactness (see Buffrénil et al. 2008). The humeri and radius show the lowest

values (<20%). It is evident from the RBT indices that the appositional growth of these long bones varies within the same individual. The low humeral RBTs suggest that these bones could not be used for digging (Ray & Chinsamy 2004). In a fossorial lifestyle the forelimbs are mainly used for digging, as a consequence the cortical bone becomes thicker increasing its RBT (Botha & Chinsamy 2004, Ray & Chinsamy 2004). The low RBT indices presented here in the forelimbs, therefore point to a non-fossorial behaviour for *Araripemys barretoi*.

In the MPSC R 010 ulna, pachyosteosclerosis indicates a local increase in bone density that is associated with a highly compacted carapace and improves the body trim and stability of *Araripemys barretoi* (Taylor 2000). However, the pachyosteosclerotic condition does not necessarily indicate a fully aquatic lifestyle for Testudines and their relatives. Amphibious and terrestrial turtles also sometimes show a high compactness of the long bones (Laurin et al. 2011, Schoch et al. 2019).

### *Skeletochronology in long bones: ontogeny and sexual maturity*

Among the osteohistological features that reflect ontogeny presented by MPSC R 010 are the high number of LAGs, and the thin zones deposited towards the periosteal margin. Similar features have already been recorded in samples of the podocnemidid *Podocnemis expansa* (Schweigger, 1812) (Chinsamy & Valenzuela 2008) and the chelid *Yaminuechelys maior* (Staesche, 1929) (Pereyra et al. 2020). The counting of LAGs could be a good method for estimating the age of an individual. As the number increases, specimens reach older ontogenetic stages, allowing us to infer the actual age of the animal (Snover & Hohn 2004). Among the studied elements the ulna preserves the greatest amount of growth marks. We attribute thus a late ontogenetic stage for the MPSC R 010 and an age of 12 years old at death is estimated for this specimen. Supplemental LAGs were not considered in our analysis, these lines are less distinct and do not appear around the entire circumference of the bone section. Their presence is related to temporary stressful environmental conditions (Snover & Hohn 2004), an environmental condition that fits the proposal for the Romualdo Formation (Almeida-Lima et al. 2020, Melo et al. 2020).

The ulna of MPSC R 010 shows a change in its growth rate between the fourth and tenth years of life, featured by a decrease and a consecutive increase in growth rate. This change in growth dynamic was considered by Pereyra et al. (2020) to be probably related to the attainment of sexual maturity in *Hydromedusa tectifera* Cope, 1869. However, the authors indicated that the subsequent increase in growth rate may be caused by other factor instead the sexual maturation. Assuming that sexual maturity was reached between 4–10 years of age by MPSC R 010 it is similar to males of Australian chelids which reached their maturity at the same age range (Spencer 2002). Different species of the chelid *Hydromedusa* show distinct age range when obtaining their sexual maturity such as 8–12 years old (in *Hydromedusa tectifera*; Pereyra et al. 2020) or 11–16 years of age (in *Hydromedusa maximilliani* (Mikan, 1825); Martins & Souza 2008). The podocnemidid *Podocnemis erythrocephala* (Spix, 1824) attained its sexual maturity at nine years of life in both genders (Bernhard, unpublished data). Carapace length is another criterion that can accompany the analysis of long bones. Hofmeyr & Fritz (2018) observed that the pelomedusid *Pelomedusa galeata* (Schoepff, 1792) achieves its sexual maturity when the shell reaches a range from 110 to 160 mm in length. Following this trend the straight carapace length of MPSC R 010 (205 mm) is higher than the length considered for other mature turtles, corroborating the skeletochronological analysis of the ulna. Comparisons with other pelomedusoids and chelids indicate that MPSC R 010 reaches its sexual maturity between 4–10 years old. Moreover,

it was at least 12 years old (based on the ulna which recorded the largest number of LAGs) before its death as evidenced by the presence of twelve LAGs. Finally, there is no evidence of an External Fundamental System (EFS), i.e., a rapid and successive deposition of growth marks at the periphery of the cortex, neither in the costal plate nor in the long bones sampled. The absence of this microstructural feature suggests that both individuals did not reach their skeletal maturity yet (Botha & Botha 2019).

## CONCLUSIONS

*Araripemys barretoi* exhibits a terrestrial histological type according to Jannello et al. (2020) contrasting with the lacustrine and marine deposits where the species has been found. This histological pattern is probably more related to the functional role increasing shell resistance to compensate its weakness caused by several fontanelles.

Considering the histological features *Araripemys* was a slow swimmer and a skilled diver, which could be submerged for short-terms. Additionally, thick and compact cortices increase the carapace's rigidity to prevent biomechanical damage. This discrepancy could be explained by an aquatic species with two extreme specializations in microanatomy of different parts of the skeleton (namely, in shell bones and in long bones; a view accepted herein) already reported in aquatic turtles (Skutschas et al. 2017). The growth strategy of *A. barretoi* suggests a moderate to slow growth rate shown by the parallel-fibred and lamellar bone tissues. As reported on other extinct and extant Testudines, *A. barretoi* attained its sexual maturity before reaching skeletal maturity, between the fourth and tenth years of age.

### Acknowledgments

We would like to express our gratitude to Dr. Diogenes de Almeida Campos who dedicated his life to the protection of Araripe fossils, inspiring our careers. We thank Professors Sandra Barreto, Lauro Santos and Virginio Neumann, who generously permitted analyses in the Laboratório de Gemologia (LABGEM/UFPE) and Laboratório Integrado de Tecnologia em Petróleo, Gás e Biocombustíveis (LITPEG/UFPE). We are also indebted to Pavel Skutschas and three anonymous reviewers for their helpful comments on the earlier version of this manuscript. Technical support for this research was provided by Charlisson Silva who performed UFRPE 5302 cross-section, Rafael Cavalcanti for previous chemical preparation of the specimens and William Alexandre for technical assistance helping us with equipment setup and procedures. This manuscript presents partial results of the doctoral thesis of the MVAS. This project was partially supported by Conselho Nacional de Desenvolvimento Científico e Tecnológico (CNPq no. 311715/2017-6 and 314222/2020-0 to JMS), Fundação Cearense de Apoio ao Desenvolvimento Científico e Tecnológico (FUNCAP #BMD-0124-00302.01.01/19 to RAMB and #BP3-013900202.0100/18 to AAFS) and the Coordenacão de Aperfeiçoamento de Pessoal de Nível Superior (finance code 001 CAPES #88887.162865/2018-00 to RAMB).

## REFERENCES

ALMEIDA-LIMA DS, PIOVESAN EK, SAYÃO JM & LIMA FJ. 2020. Description and ontogeny of *Pattersoncypris minima* sp. nov. (Crustacea: Ostracoda), Araripe Basin, Northeast Brazil. Zootaxa 4851: 171-179.

ARAI M & ASSINE ML. 2020. Chronostratigraphic constraints and paleoenvironmental interpretation of the Romualdo Formation (Santana Group, Araripe Basin, Northeastern Brazil) based on palynology. Cretac Res 116: 104610.

ASSINE ML, PERINOTTO JAJ, CUSTÓDIO MA, NEUMANN VH, VAREJÃO FG & MESCOLOTTI PC. 2014. Sequências deposicionais do Andar Alagoas da Bacia do Araripe, Nordeste do Brasil. Bol Geocienc Petrobras 22: 3-28.

BALANI K, PATEL RR, KESHRI AK, LAHIRI D & AGARWAL A. 2011. Multi scale hierarchy of *Chelydra serpentina*: Microstructure and mechanical properties of turtle shell. J Mech Behav Biomed Mater 4: 1440-1451.

BENIGNO ANA, SARAIVA AÁ, SIAL AN & LACERDA LD. 2021. Mercury chemostratigraphy as a proxy of volcanic-driven environmental changes in the Aptian-Albian transition, Araripe Basin, northeastern Brazil. J S Am Earth Sci 107: 103020.

BHAT MS, CHINSAMY A & PARKINGTON J. 2019. Long bone histology of *Chersina angulata*: Interelement variation and life history data. J Morphol 280: 1881-1899.

BOTHA AE & BOTHA J. 2019. Ontogenetic and inter-elemental osteohistological variability in the leopard tortoise *Stigmochelys pardalis*. PeerJ 7: e8030.

BOTHA J & CHINSAMY A. 2004. Growth and life habits of the Triassic cynodont *Trirachodon*, inferred from bone histology. Acta Palaeontol Pol 49: 619-627.

BUFFRÉNIL V, ASTIBIA H, PEREDA SUBERBIOLA X, BERRETEAGA A & BARDET N. 2008. Variation in bone histology of middle Eocene sirenians from western Europe. Geodiversitas 30: 425-432.

CARVALHO ARA & BARRETO AMF. 2015. Novos Materiais de *Araripemys barretoi* da Formação Romualdo (Albiano - Bacia do Araripe), Pernambuco, Brasil. Estud Geol 25: 3-14.

CERDA IA, POL D & CHINSAMY A. 2014. Osteohistological insight into the early stages of growth in *Mussaurus patagonicus* (Dinosauria, Sauropodomorpha). Hist Biol 26: 110-121.

CERDA IA, STERLI J & SCHEYER TM, 2016. Bone shell microstructure of *Condorchelys antiqua* Sterli, 2008, a stem turtle from the Jurassic of Patagonia. Comptes Rendus Palevol 15: 128-141.

CHINSAMY A & RAATH M. 1992. Preparation of fossil bone for histological examination. Palaeontol Africana 29: 39-44.

CHINSAMY A & VALENZUELA N. 2008. Skeletochronology of the endangered side neck turtle, *Podocnemis expansa*. S Afr 104: 311-314.

CLARAC F, SCHEYER TM, DESOJO JB, CERDA IA & SANCHEZ S. 2020. The evolution of dermal shield vascularization in Testudinata and Pseudosuchia: phylogenetic constraints versus ecophysiological adaptations. Phil Trans R Soc B 375: 20190132.

DANILOV IG, OBRAZTSOVA EM, BOITSOVA EA & SKUTSCHAS PP. 2018. Diversity of Middle Jurassic turtles from the Berezovsk Quarry Locality, Krasnoyarsk Region, Russia: morphology and histological study. Paleontol J 52: 188-200.

DE LA FUENTE M, MANIEL I, JANNELLO J, STERLI J, GARRIDO A, GARCÍA R, SALGADO L, CANUDO J & BOLATTI R. 2017. Unusual shell anatomy and osteohistology in a new Late Cretaceous panchelid turtle from northwestern Patagonia, Argentina. Acta Palaeontol Pol 62: 585-601.

ENLOW DH. 1962. A study of the post-natal growth and remodelling of bone. Am J Anat 110: 79-101.

ENLOW DH. 1963. Principles of bone remodeling: an account of post-natal growth and remodeling processes in the long bones and the mandible. Springfield: Charles Thomas.

FRANCILLON-VIEILLOT H, DE BUFFRÉNIL V, CASTANET J, GÉRAUDIE J, MEUNIER FJ, SIRE JY, ZYLBERBERG L & DE RICQLÈS A. 1990. Microstructure and mineralization of vertebrate skeletal tissues. In: Carter JG (Ed), Skeletal Biomineralization: Patterns, Processes and Evolutionary Trends, New Jersey: Van Nostrand Reinhold, New York, USA, p. 471-548.

GILBERT SF, LOREDO GA, BRUKMAN A & BURKE AC. 2001. Morphogenesis of the turtle shell: the development of a novel structure in tetrapod evolution. Evol Dev 3: 47-58.

GIRONDOT M & LAURIN M. 2003. Bone profiler: A tool to quantify, model, and statistically compare bone-section compactness profiles. J Vertebr Paleontol 23: 458-461.

HOFMEYR MD & FRITZ U. 2018. *Pelomedusa galeata*. The IUCN Red List of Threatened Species, published in 2019. doi.org/10.2305/IUCN.UK.2018 2.RLTS.T113551736A144762886.en

HOUSSAYE A. 2013. Bone histology of aquatic reptiles: What does it tell us about secondary adaptation to an aquatic life? Biol J Linn Soc 108: 3-21.

JANNELLO JM, CERDA IA & DE LA FUENTE MS. 2016. Shell bone histology of the long-necked chelid *Yaminuechelys* (Testudines: Pleurodira) from the Late Cretaceous—Early Palaeocene of Patagonia with comments on the histogenesis of bone ornamentation. Sci Nat 103: 1-11.

JANNELLO JM, CERDA IA & DE LA FUENTE MS. 2020. The relationship between bone shell microanatomy and palaeoecology in Testudinata from South America. Palaeogeogr Palaeoclimatol Palaeoecol 537: 109412.

KRILOFF A, GERMAIN D, CANOVILLE A, VINCENT P, SACHE M & LAURIN M. 2008. Evolution of bone microanatomy of the tetrapod tibia and its use in palaeobiological inference. J Evol Biol 21: 807-826.

KELLNER AWA, CAMPOS DA, SAYÃO JM, SARAIVA AAS, RODRIGUES T, OLIVEIRA G, CRUZ LA, COSTA FR, SILVA HP & FERREIRA JS. 2013. The largest flying reptile from Gondwana: a new specimen of Tropeognathus cf. T. mesembrinus Wellnhofer, 1987 (Pterodactyloidea, Anhangueridae) and other large pterosaurs from the Romualdo Formation, Lower Cretaceous, Brazil. An Acad Bras Cienc 85: 113-135.

LAMM ET. 2013. Preparation and sectioning of specimens. In: Padian K & Lamm ET (Eds), Bone Histology of Fossil Tetrapods: Advancing Methods, Analysis, and Interpretation, Berkeley: University of California Press, California, USA, p. 55-160.

LANDBERG T. 2003. Lung ventilation during treadmill locomotion in a terrestrial turtle, *Terrapene carolina*. J. Exp. Biol 206: 3391-3404.

LAURIN M, CANOVILLE A & GERMAIN D. 2011. Bone microanatomy and lifestyle: A descriptive approach. C R Palevol 10: 381-402.

LIMAVERDE S, PÊGAS RV, DAMASCENO R, VILLA C, OLIVEIRA GR, BONDE N & LEAL MEC. 2020. Interpreting character variation in turtles: *Araripemys barretoi* (Pleurodira: Pelomedusoides) from the Araripe Basin, Early Cretaceous of Northeastern Brazil. PeerJ 8: e9840.

LYSON T, RUBIDGE BS, SCHEYER TM, QUEIROZ K, SCHACHNER ER, SMITH RMH, BOTHA-BRINK J & BEVER GS. 2016. Fossorial origin of the turtle shell. Curr Biol 26: 1887-1894.

MARTILL DM. 2007. The age of the Cretaceous Santana Formation fossil Konservat Lagerstätte of north-east

Brazil: a historical review and an appraisal of the biochronostratigraphic utility of its palaeobiota. Cretac Res 28: 895-920.

MARTILL DM, LOVERIDGE RF & HEIMHOFER U. 2007. Halite pseudomorphs in the Crato Formation (Early Cretaceous, Late Aptian-Early Albian), Araripe Basin, Northeast Brazil: further evidence for hypersalinity. Cretac Res 28: 613-620.

MARTINS FI & SOUZA FL. 2008. Estimates of growth of the Atlantic Rain Forest freshwater turtle *Hydromedusa maximiliani* (Chelidae). J Herpetol 42: 54-60.

MELO RM, GUZMÁN J, ALMEIDA-LIMA D, PIOVESAN EK, NEUMANN VH & SOUSA AJ. 2020. New marine data and age accuracy of the Romualdo Formation, Araripe Basin, Brazil. Sci Rep 10: 1-15.

MEYLAN PA. 1996. Skeletal morphology and relationships of the Early Cretaceous side-necked turtle, *Araripemys barretoi* (Testudines: Pelomedusoides: Araripemydidae), from the Santana Formation of Brazil. J Vertebr Paleontol 16: 20-33.

NEUMANN VH, BORREGO AG, CABRERA L & DINO R. 2003. Organic matter composition and distribution through the Aptian-Albian lacustrine sequences of the Araripe Basin, northeastern Brazil. Int J Coal Geol 54: 21-40.

OLIVEIRA GR & KELLNER AWA. 2005. Note on a plastron (Testudines, Pleurodira) from the lower cretaceous Crato member, Santana formation, Brazil. Arq Mus Nac 63: 523-528.

OLIVEIRA GR & KELLNER AWA. 2017. Rare hatchling specimens of *Araripemys* Price, 1973 (Testudines, Pelomedusoides, Araripemydidae) from the Crato Formation, Araripe Basin. J South Am Earth Sci 79: 137-142.

OLIVEIRA GR & ROMANO PSR. 2007. Histórico dos achados de tartarugas fósseis do Brasil. Arch Mus Nac 65: 113-133.

OLIVEIRA GR, SARAIVA AÁF, SILVA HP, ANDRADE JAFG & KELLNER AWA. 2011. First turtle from the Ipubi Formation (Early Cretaceous), Santana Group, Araripe Basin, Brazil. Rev Bras Paleontol 14: 61-66.

PEREYRA ME, BONA P, CERDA I, JANNELLO J, DE LA FUENTE M & DESÁNTOLO B. 2020. Growth dynamics and body size evolution of South American long-necked chelid turtles: a bone histology approach. Acta Palaeontol Pol 65: 535-545.

PRICE LI. 1973. Quelônio Amphichelydia no Cretáceo Inferior do Nordeste do Brasil. Rev Bras Geoc 3: 84-96.

RAY S & CHINSAMY A. 2004. *Diictodon feliceps* (Therapsida, Dicynodontia): bone histology, growth, and biomechanics. J Vertebr Paleontol 24: 180-194.

ROMANO PSR, OLIVEIRA GR, AZEVEDO SAK, KELLNER AWA & CAMPOS DA. 2013. New information about the Pelomedusoides (Testudines: Pleurodira) from the Cretaceous of Brazil. In: Brinkman DB, Holroyd PA & Gardner JD (Eds), Morphology and Evolution of Turtles: Origin and Early Diversification. Springer, Dordrecht, Netherlands, p. 261-275.

SCHEYER TM, DANILOV IG, SUKHANOV VB & SYROMYATNIKOVA EV. 2014. The shell bone histology of fossil and extant marine turtles revisited. Biol J Linn Soc Lond 112: 701-718.

SCHEYER TM, SANDER MP, JOYCE WG, BÖHME W & WITZEL U. 2007. A plywood structure in the shell of fossil and living soft-shelled turtles (Trionychidae) and its evolutionary implications. Org Divers Evol 7: 136-144.

SCHEYER TM, PÉREZ-GARCÍA A & MURELAGA X. 2015. Shell bone histology of solemydid turtles (stem Testudines): palaeoecological implications. Org Divers Evol 15: 199-212.

SCHEYER TM & SÁNCHEZ-VILLAGRA MR. 2007. Carapace bone histology in the giant pleurodiran turtle *Stupendemys geographicus*: Phylogeny and function. Acta Palaeontologica Polonica 52: 137-154.

SCHEYER TM & SANDER PM. 2007. Shell bone histology indicates terrestrial palaeoecology of basal turtles. Proceedings of the Royal Society of London B 274: 1885-1893.

SCHINDELIN J ET AL. 2012. Fiji: An open-source platform for biological-image analysis. Nat Methods 9: 676-682.

SCHOCH RR, KLEIN N, SCHEYER TM & SUES HD. 2019. Microanatomy of the stem-turtle *Pappochelys rosinae* indicates a predominantly fossorial mode of life and clarifies early steps in the evolution of the shell. Sci Rep 9: 1-10.

SENA MVA, BANTIM RAM, SARAIVA AÁF, SAYÃO JM & OLIVEIRA GR. 2021. Osteohistology and microanatomy of a new specimen of *Cearachelys placidoi* (Testudines: Pleurodira) a side-necked turtle from the Lower Cretaceous of Brazil. Anat Rec 1-11.

SILVA SANTOS RD & VALENÇA JGA. 1968. A Formação Santana e sua paleoictiofauna. An Acad Bras Cienc 40: 339-360.

SKUTSCHAS PP, BOITSOVA EA, CHEREPANOV GO, DANILOV IG. 2017. Shell bone histology of the pan-carettochelyid turtle *Kizylkumemys schultzi* from the Upper Cretaceous of Uzbekistan and shell bone morphology transformations in the evolution of pan-trionychian turtles. Cretac Res 79: 171-181.

SNOVER ML & HOHN AA. 2004. Validation and interpretation of annual skeletal marks in loggerhead (*Caretta caretta*) and Kemp's ridley (*Lepidochelys kempii*) sea turtles. Fish Bull 102: 682-692.

SNOVER ML, HOHN AA, GOSHE LR & BALAZS GH. 2011. Validation of annual skeletal marks in green sea turtles *Chelonia mydas* using tetracycline labeling. Aquat Biol 12: 197-204.

SPENCER RJ. 2002. Growth patterns of two widely distributed freshwater turtles and a comparison of common methods used to estimate age. Aust J Zool 50: 477-490.

TAYLOR M. 2000. Functional significance of bone ballastin in the evolution of buoyancy control strategies by aquatic tetrapods. Hist Biol 14: 15-31.

VALENÇA LMM, NEUMANN VH & MABESOONE JM. 2003. An overview on Callovian Cenomanian intracratonic basins of Northeast Brazil: Onshore stratrigraphic record of the opening of the southern Atlantic. Geol Acta 1: 261-275.

VIEIRA LG, SANTOS ALQ, MOURA LR, ORPINELLI SRT, PEREIRA KF & LIMA FC. 2016. Morphology, development and heterochrony of the carapace of Giant Amazon River Turtle, *Podocnemis expansa* (Testudines, Podocnemidae). Pesq Vet Bras 36: 436-446.

WANG X, HUANG Y, ZHONG M, YANG S, YANG X, JIANG J & HU J. 2019. Environmental stress shapes life-history variation in the swelled-vented frog (*Feirana quadranus*). Evol Ecol 33: 435-448.

WOODWARD HN, RICH TH & VICKERS-RICH P. 2018. The bone microstructure of polar "hypsilophodontid" dinosaurs from Victoria, Australia. Sci Rep 8: 1162.

WYNEKEN J. 2001. The Anatomy of Sea Turtles, Miami: National Marine Fisheries Service, National Oceanic and Atmospheric Administration, US Department of Commerce, 172 p.

## SUPPLEMENTARY MATERIAL

**Figure S1. Schematic black (bone) and white (vascular spaces and medullary cavities) drawings of the extinct *Araripemys barretoi* prepared for use with Bone Profiler. a, Perpendicular section of costal V plate (MPSC R 010). b, Parallel section of costal V plate (MPSC R 010). c, Perpendicular section of the neural V plate (UFRPE 5302). d, Transversal section of a peripheral plate (MPSC R 010). e, Transversal section of humeral epiphysis (MPSC R 010). f, Transversal section of ulna (MPSC R 010). g, Transversal section of humeral metaphysis (MPSC R 010). h, Transversal section of radius (MPSC R 010). i-l, Transversal sections of metapodials (MPSC R 010), metatarsal I (i); metatarsal II (j); metatarsal III (k); and metatarsal IV (l).**

**How to cite**

SENA MVA, BANTIM RAM, SARAIVA AAF, SAYÃO JM & OLIVEIRA GR. 2021. Shell and long-bone histology, skeletochronology, and lifestyle of Araripemys barretoi (Testudines: Pleurodira), a side-necked turtle of the Lower Cretaceous from Brazil. An Acad Bras Cienc 93: e20201606. DOI 10.1590/0001-3765202120201606.

*Manuscript received on October 6, 2020;*
*accepted for publication on March 12, 2021*

**MARIANA VALÉRIA A. SENA**[1,2]
https://orcid.org/0000-0003-4708-999X

**RENAN ALFREDO M. BANTIM**[3]
https://orcid.org/0000-0003-4576-0989

**ANTÔNIO A.F. SARAIVA**[3]
https://orcid.org/0000-0003-0127-8912

**JULIANA M. SAYÃO**[4]
https://orcid.org/0000-0002-3619-0323

**GUSTAVO R. OLIVEIRA**[5]
https://orcid.org/0000-0002-9871-1235

[1]Universidade Federal de Pernambuco, Programa de Pós-Graduação em Geociências (PPGEOC), Departamento de Geologia, Avenida Prof. Moraes Rego, 1235, Cidade Universitária, 50670-901 Recife, PE, Brazil

[2]Centro Universitário da Vitória de Santo Antão, Loteamento São Vicente Ferrer, 71, Cajá, 55610-050 Vitória de Santo Antão, PE, Brazil

[3]Universidade Regional do Cariri, Laboratório de Paleontologia da URCA, Rua Carolino Sucupira, s/n, Pimenta, 63105-000 Crato, CE, Brazil

[4]Universidade Federal do Rio de Janeiro, Laboratório de Paleobiologia e Paleogeografia Antártica, Museu Nacional, Quinta da Boa Vista s/n, São Cristóvão, 20940-040 Rio de Janeiro, RJ, Brazil

[5]Universidade Federal Rural de Pernambuco, Laboratório de Paleontologia & Sistemática, Departamento de Biologia, Rua Dom Manoel de Medeiros, s/n, Dois Irmãos, 52171-900 Recife, PE, Brazil

**Correspondence to**: Mariana Valéria de Araújo Sena
*E-mail: mari.araujo.sena@gmail.com*

## Author contributions

MVAS – Conceived the idea and planned the analyses; performed the analyses and wrote the manuscript. RAMB – Contributed to the interpretation of the results and wrote the manuscript. AAFS – Collected the specimens; contributed to the interpretation of the results and wrote the manuscript. JMS – Assisted with data and analyses; helped supervise the project and wrote the manuscript. GRO – Conceived and planned the analyses; supervised the findings of this work and wrote the manuscript.

All authors discussed the results and contributed to the final manuscript.